Supplementary Information

π-Conjugation Effect Influenced the Oxygen Electrochemical Reaction Electrochemical Efficiency in Fe-N-C Catalysts

Xiaoqi Zhao, Xue Zhang, ZhiPeng Li, Ziyue Wang, Zihan Guo*, Yanfang Gao**

(School of Chemical Engineering, Inner Mongolia University of Technology, Huhhot 010051, China;

Engineering Research Center of Large Energy Storage Technology, Inner Mongolia University of Technology, Huhhot 010051, China)

Corresponding Authors:

Email addresses: *gzh@imut.edu.cn* (Zihan Guo*); *yf_gao@imut.edu.cn* (Yanfang Gao**)

Details of Experiments and Methods

Medicine

Specifically, anhydrous zinc chloride ($ZnCl_2$), pyromellitic dianhydride (PMDA, ≥99 %), 1,4,5,8-naphthalenetetracarboxylic dianhydride (NTCDA, 96%), Perylene-3,4,9,10-tetracarboxylic dianhydride (PTCDA, 98%), and melamine (MA, 99%) were bought from Mreda company. Nafion solvents (~ 5% in a mixture of lower aliphatic alcohols and water) were obtained from Macklin manufacturers. KOH (analytically pure), anhydrous ethanol, and tetrahydrofuran (analytically pure) were purchased from Fuchen (Tianjin) Chemical Reagent Co., Ltd. Distilled water was produced in the laboratory.

Physical characterization

^{13}C NMR spectra were required by using the solid-state nuclear magnetic resonance spectrometer (Bruker 400 M) produced in Germany at a resonance frequency of 400 MHz. FT-IR with 400 cm^{-1} ~ 4000 cm^{-1} was obtained from the Fourier transform infrared spectrometer (IRTRACER-100) made in Shimadzu, Japan. Before the test, KBr was vacuum dried at 70 °C for 4 h, and the mass ratio of KBr to sample was 100:1. Solid-state cross-polarization magic angle spinning (CP/MAS) The XRD patterns were tested by using the X-ray diffractometer (miniflex 600) produced by Rigaku of Japan in the range of $2\theta = 0 \sim 50°$ and $0 \sim 90°$ at the scanning rate of $10°\cdot min^{-1}$. The degree of graphitization of the prepared catalysts was analyzed by the Raman spectrum obtained by the INVIA REFLEX laser micro-Raman spectrometer produced by Renishaw Company in the United Kingdom under the excitation

wavelength of 532 nm and the condition of 500 cm^{-1} ~ 4000 cm^{-1}. The Hitachi Regulus 8220 cold field emission scanning electron microscope (Field Emission Scanning Electron Microscope, Hitachi, Japan) was used to obtain SEM images and EDS mapping results at different sizes. The isothermal N_2 adsorption and desorption curves were obtained at 77.3 K by using the Autosorb-IQ-MP gas adsorption analyzer produced by the American Conta Company. Before the test, the programmed temperature was used to degas at 80°C for 60 min, at 150°C for 60 min, and at 300°C for 180 min. The XPS spectra of the prepared samples were obtained by X-ray photoelectron spectroscopy (ESCALAB 250 Xi) X-ray photoelectron spectroscopy produced by Thermo-Fisher Company in the United States.

Synthetic procedures of *x*CN catalysts

1 mmol dianhydride, 2 mmol MA, and 8.4 mmol $ZnCl_2$ were weighed and ground in an agate grinding bowl for 30 min. Then, the mixture was heated at 315 °C for 8 h in N_2. The obtained solids were freeze-dried for 24 h after being washed three times with 0.1 $mol \cdot L^{-1}$ HCl, tetrahydrofuran, and distilled water, respectively. The dried solids were *x*CN catalysts. The *x*CN catalysts were named SPCN when PMDA was selected for dianhydride, the MNCN catalysts were obtained when NTCDA was applied, and the LBCN catalysts were synthesized when PTCDA was used.

Synthetic procedures of *x*CN/Fe catalysts

50 mL of 0.08 $mol \cdot L^{-1}$ $Fe(NO_3)_3 \cdot 9H_2O$ aqueous solution was mixed with 300 mg *x*CN catalysts and stirred for 72 h. Then, they were freeze-dried for 24 h after being centrifuged. The final *x*CN/Fe catalysts were obtained after pyrolysis at 900 °C for 3 h

in N_2.

Electrochemical test

4 mg *x*CN/Fe catalysts were added to 1000 μL dispersion, which was prepared by mixing 250 μL ethanol and 750 μL distilled water. After ultrasonication for 20 min, 20 μL Nafion was added and then ultrasonicated for another 20 min to form an ink-like slurry. At the same time, the rotating disc ring electrode (RRDE) was polished with 0.05 μm Al_2O_3 powder. Take 20 μL of the ink-like slurry and apply it to the surface of the RRDE, and wait for it to be completely dry. The ORR electrocatalytic performance of the samples was tested in 0.1 $mol \cdot L^{-1}$ KOH aqueous solution with Pt wire as the counter electrode, Ag/AgCl as the reference electrode, and the RRDE loaded with catalyst as the working electrode. During the test, the alkaline electrolyte was first purged with N_2 for 40 min until it was saturated. The CV curves were cycled for 50 cycles at a scan rate of 50 $mV \cdot s^{-1}$ in the voltage range of -1 ~ 0.2 V *vs.* Ag/AgCl. After that, O2 was introduced into the electrolyte for 20 min until saturation. The LSV polarization curves at different speeds (400 rpm, 800 rpm, 1,200 rpm, 1,600 rpm, 2,000 rpm, and 2,400 rpm) were obtained at a scan rate of 5 $mV \cdot s^{-1}$ in the same voltage range. The stability of the electrocatalysts was obtained by testing the LSV polarization curves of the catalysts at a scan rate of 5 $mV \cdot s^{-1}$ in the voltage range of -1 ~ 0.2 V *vs.* Ag/AgCl after 3,000 cycles of CV curves at a scan rate of 50 $mV \cdot s^{-1}$ in the voltage range of 0.6 ~ 1.0 V *vs.* RHE, and comparing the LSV polarization curves before and after the cycle. The CN^- poisoning experiment of Fe-N_x active sites was carried out according to the literature.[1, 2]

Another 20 μL of the above ink-like slurry was added dropwise to the nickel foam (1 cm × 1 cm) and completely dried. The OER electrocatalytic performance of the samples was tested in 0.1 mol·L^{-1} KOH aqueous solution with a high-purity graphite carbon rod as the counter electrode, Ag/AgCl as the reference electrode, and completely dried nickel foam as the working electrode. The OER electrochemical performance tests of all catalysts were carried out on the CHI 760e electrochemical workstation. During the test, the alkaline electrolyte was first passed through 20 min of O_2 until saturation. The CV curves were cycled for 40 cycles at a scan rate of 50 mV·s^{-1} in the voltage range of 0 ~ 0.5 V *vs.* Ag/AgCl. Then, the LSV polarization curves were obtained at a scan rate of 5 mV·s^{-1} in the voltage range of-0.2 ~ 1.2 V *vs.* Ag/AgCl without i-R compensation. Subsequently, in the voltage range of 0.1 ~ 0.3 V *vs*. Ag/AgCl, the scanning rate was increased from 20 mV·s^{-1} to 200 mV·s^{-1} with a step of 20 mV·s^{-1} after 4 cycles to obtain CV curves at different scanning rates. The stability of the catalysts was obtained by testing the LSV polarization curve in -0.2 ~ 1.2 V *vs.* Ag/AgCl after 3,000 cycles of CV curves in the voltage range of 0.1 ~ 0.3 V vs. Ag/AgCl, and comparing the LSV polarization curves before and after the cycle. The i-t curve was obtained by chronoamperometry at a voltage of 1.52 V vs. Ag/AgCl for 36,000 s.

The catalysts prepared by 8 mg were dispersed into a mixed solution of 500 μL ethanol, 1,500 μL distilled water, and 40 μL Nafion solvent, and the catalyst slurry was prepared after ultrasonic treatment for 40 min. 750 μL of catalyst slurry was measured and dropped on the electrode composite substrate synthesized by

commercially purchased nickel foam and hydrophobic carbon paper to form a circular catalyst area with a diameter of 1 cm, waiting for air drying. The air-dried electrode substrate was used as the cathode electrode of the rechargeable Zn-air battery, the Zn sheet was used as the anode, and 4 mol·L^{-1} KOH was used as the electrolyte. Testing ORR/OER at a lower electrolyte concentration can provide a mild environment and reduce the reaction process of OH^- ions interfering with the electrode surface, to observe the intrinsic activity of the catalysts. The higher electrolyte concentration can provide sufficient OH^- ions for the zinc-air battery, which is conducive to the dissolution of zinc, reducing the occurrence of side reactions and improving the mass transfer and diffusion of O_2. [3, 4]

Firstly, the open circuit voltage (OCP) of two Zn-air battery devices in parallel was tested by a universal meter. Secondly, the OCP of 18,000 s was tested on the CHI 760e electrochemical workstation, and then the CV curve was tested in the voltage range of 1.4 V ~ 2.5 V. Subsequently, the LSV curve was tested in the voltage range of 1.55 ~ 0.2 V. Two Zn-air battery devices were connected in series and connected to a small bulb to observe whether the small bulb is bright. Finally, the charge-discharge electrochemical method was used to test the 1,000-cycle data at 0.0078 V at Princeton electrochemical workstation, with a cycle of charging for 10 min and then discharging for 10 min to evaluate the stability of the battery.

Square wave voltammetry experiment. Square wave voltammetry test was performed in N_2-saturated 0.1 mol·L^{-1} KOH electrolyte with a step potential of 1 mV, amplitude of 1 mV, and scan frequency of 10 Hz.

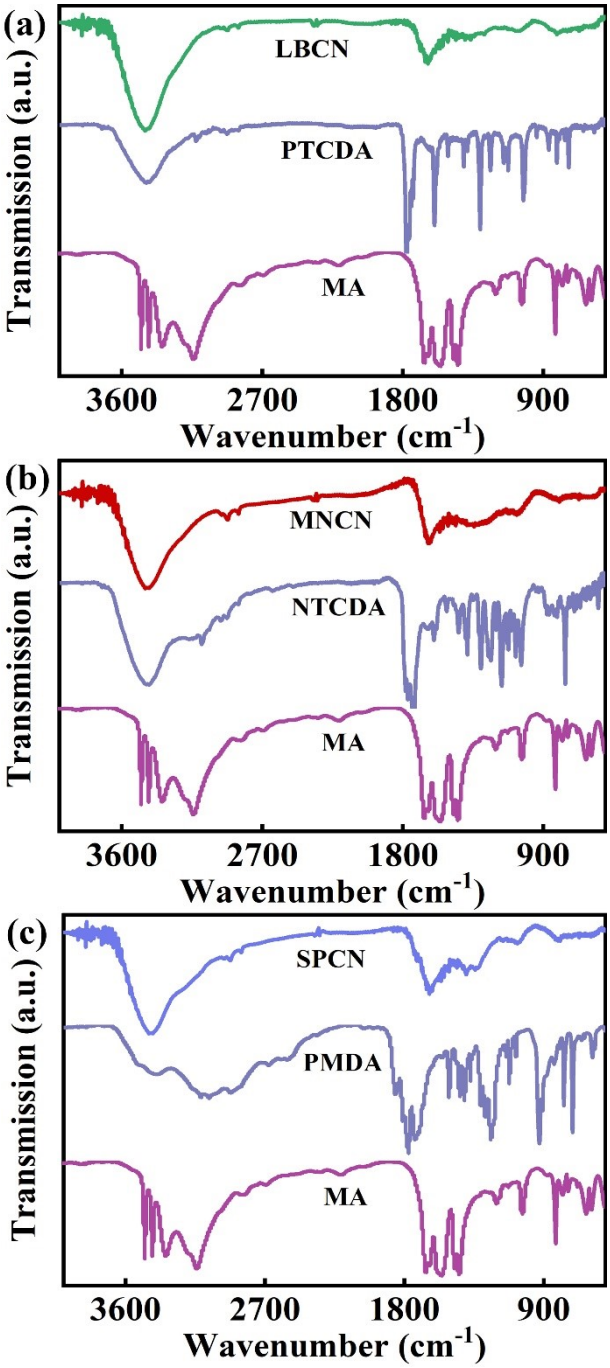

Figure S1 FT-IR spectra of *x*CN catalysts and their corresponding ligands: (a) LBCN catalysts, PTCDA, and MA; (b) MNCN catalysts, PTCDA, and MA; (c) SPCN catalysts, PTCDA, and MA.

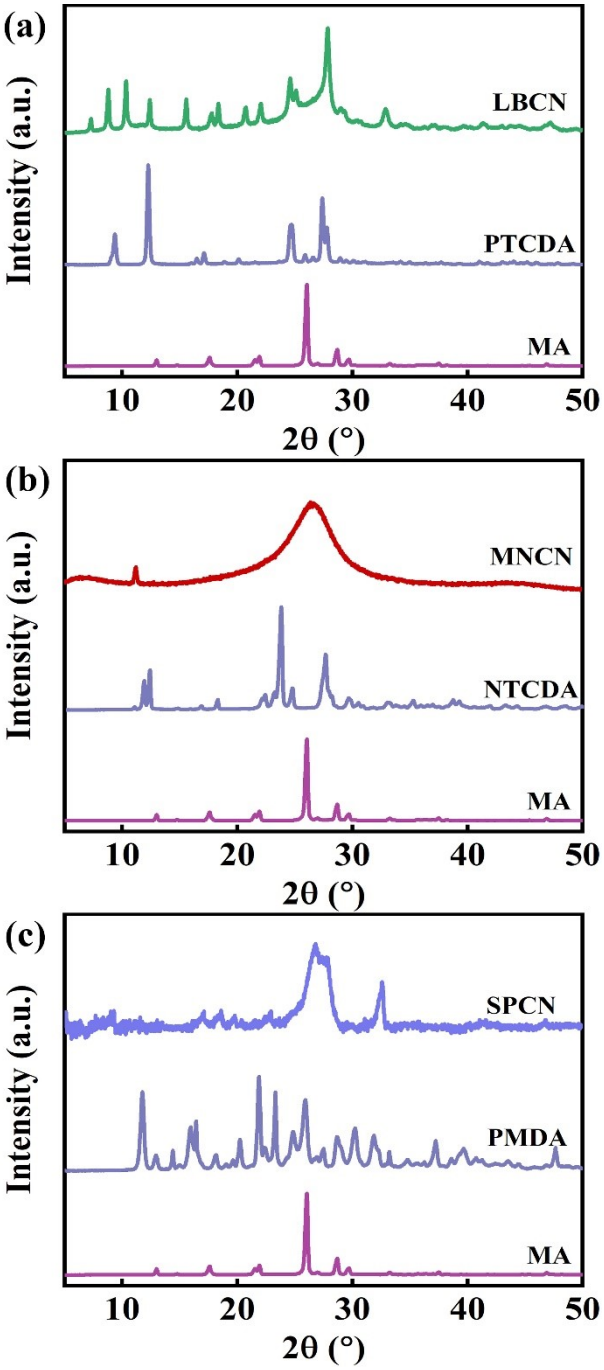

Figure S2 XRD pattern of *x*CN catalysts and their corresponding ligands: (a) LBCN catalysts, PTCDA, and MA; (b) MNCN catalysts, PTCDA, and MA; (c) SPCN catalysts, PTCDA, and MA.

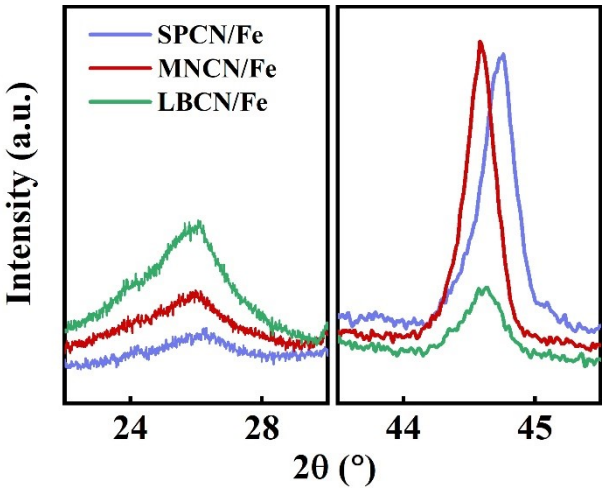

Figure S3 The enlarged XRD pattern at 2θ = 25~26˚ and 2θ = 43~46˚.

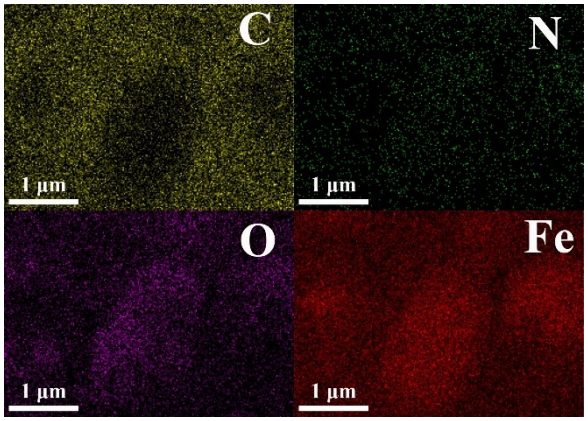

Figure S4 The EDS elemental mapping (C, N, O, Fe) images of MNCN/Fe catalysts in SEM.

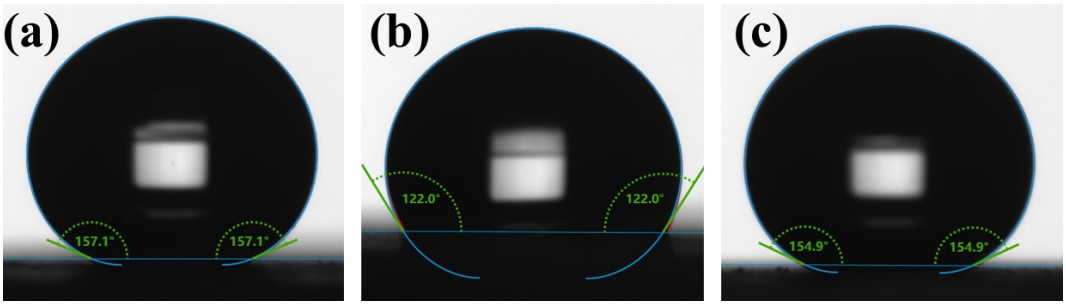

Figure S5 Contact angle of (a) SPCN/Fe, (b) MNCN/Fe and (c) LBCN/Fe catalysts. The liquid was water and the surrounding atmosphere was air.

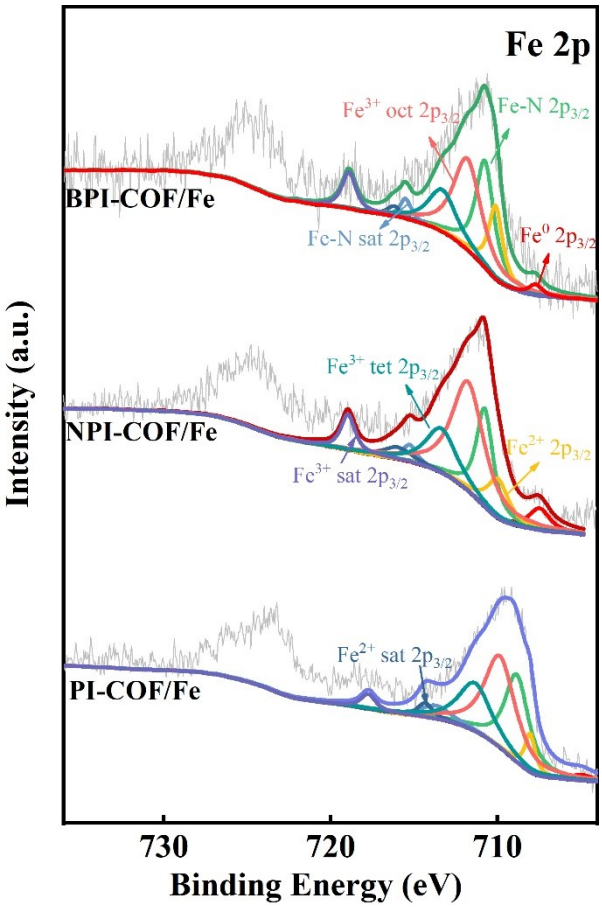

Figure S6 Fe 2p XPS spectra of *x*CN/Fe catalysts.

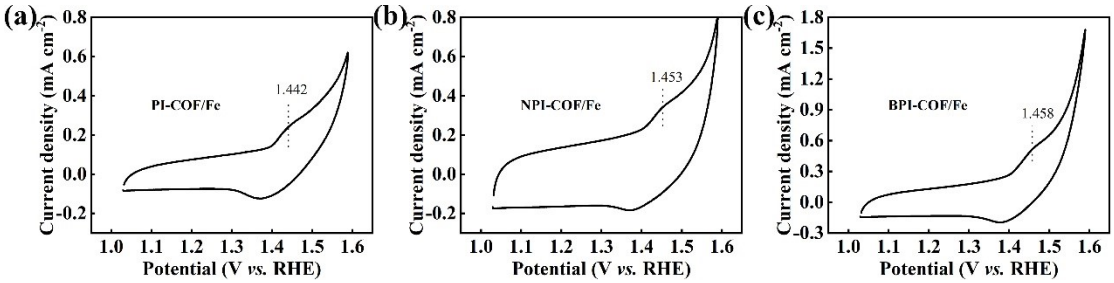

Figure S7 CV measurements of *x*CN/Fe catalysts showing Fe redox peaks.

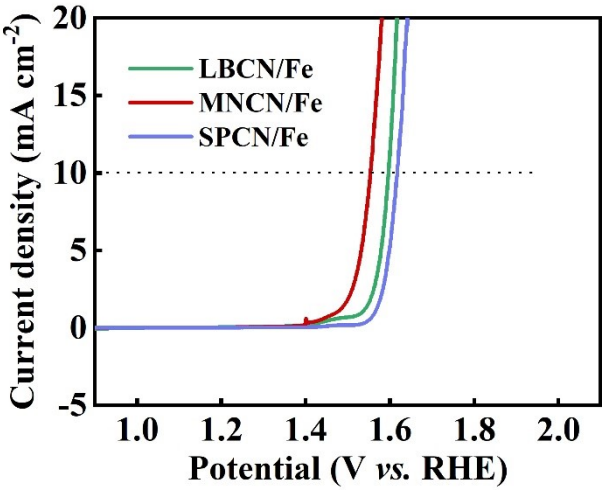

Figure S8 LSV of *x*CN/Fe catalysts after iR compensation.

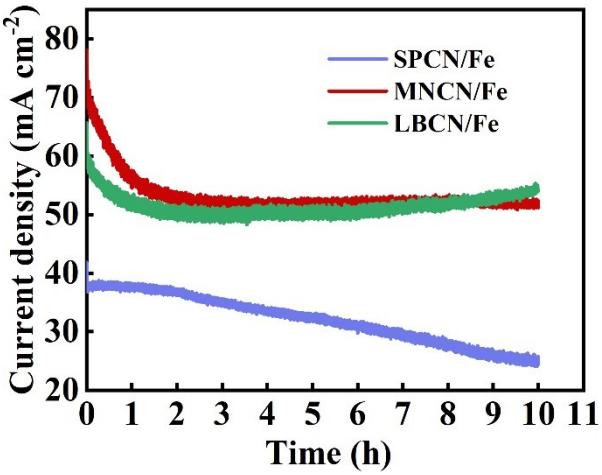

Figure S9 i-t test of *x*CN/Fe catalysts.

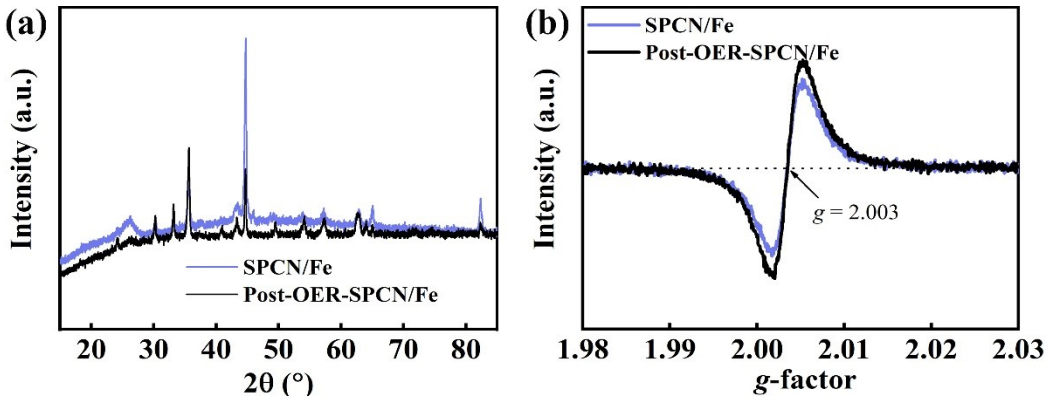

Figure S10 (a) XRD patterns and (b) EPR spectra for SPCN/Fe initially and after 10 h OER.

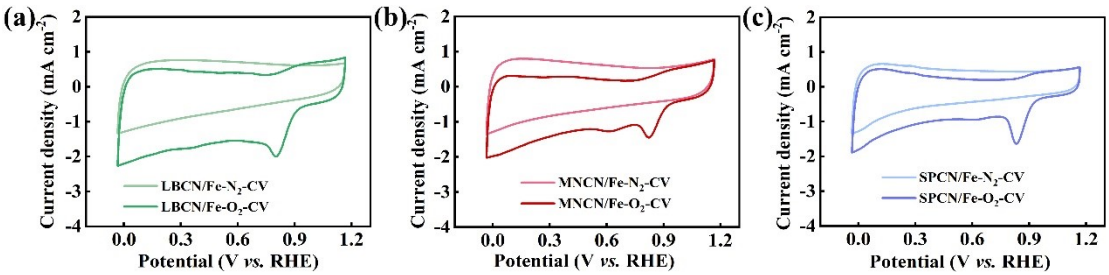

Figure S11 CV measurements of *x*CN/Fe catalysts during ORR electrocatalytic progress.

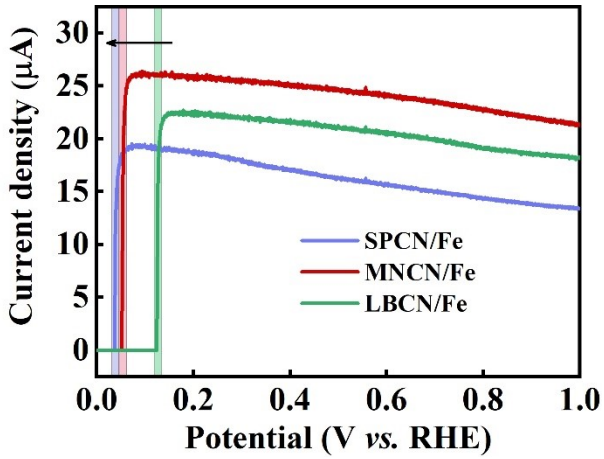

Figure S12 Square wave voltammetry (SWV) profiles of *x*CN/Fe catalysts.

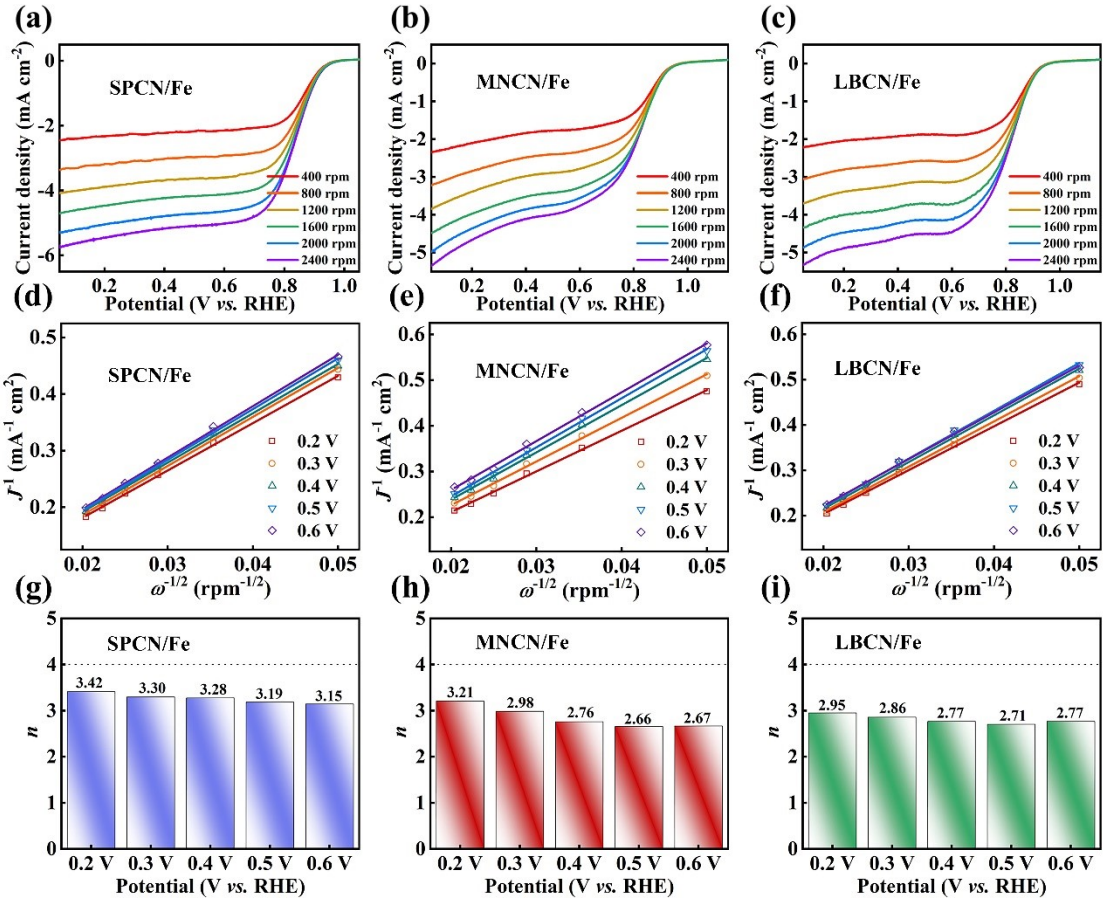

Figure S13 (a-c) LSV curves at different speeds; (d-f) K-L equation and (g-i) *n* of *x*CN/Fe catalysts.

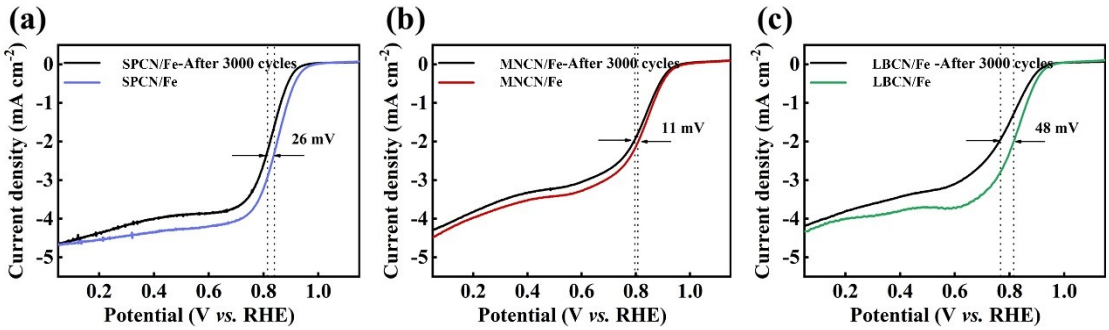

Figure S14 ORR stability test of (a) SPCN/Fe catalysts, (b) MNCN/Fe catalysts and (c) LBCN/Fe catalysts.

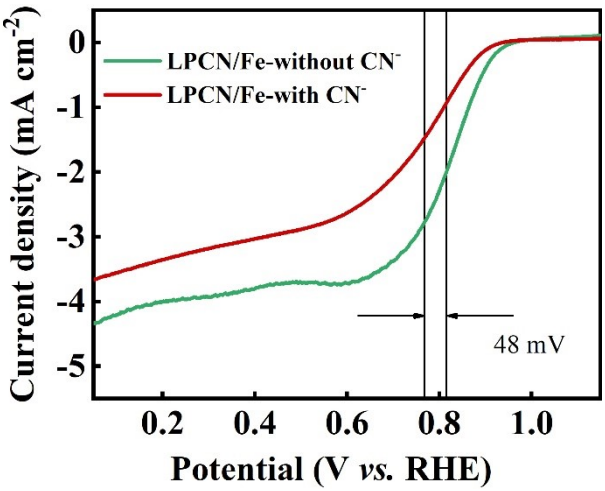

Figure S15 LSV polarization curves of LBCN/Fe catalysts in O_2-saturated 0.1 mol·L^{-1} KOH aqueous solution with CN^- and without CN^-.

Table S1 Specific surface area and pore size distribution of *x*CN/Fe catalysts.

Name	S_{BET} ($m^2 \cdot g^{-1}$)	S_{micro} ($m^2 \cdot g^{-1}$)	S_{meso} ($m^2 \cdot g^{-1}$)	V_{total} ($cm^3 \cdot g^{-1}$)	V_{mico} ($cm^3 \cdot g^{-1}$)	V_{meso} ($cm^3 \cdot g^{-1}$)	V_{mico}/V_{total}	V_{meso}/V_{total}	D_{pore} (nm)
SPCN/Fe	419.4	16.745	304.272	0.782	0.004	0.69	0.51 %	88.24 %	7.412
MNCN/Fe	187.4	149.77	47.745	0.18	0.063	0.101	35.00 %	56.11 %	3.365
LBCN/Fe	94.8	66.753	95.405	0.224	0.014	0.214	6.25 %	95.54 %	9.149

Table S2. The electrochemical performance comparison of COFs derived carbon-based catalysts with those reported in the literature under alkaline conditions.

No.	Name	η (V *vs.* RHE)	$E_{1/2}$ (V *vs.* RHE)	P_{max} ($mW \cdot cm^{-2}$)	Reference
1	MNCN/Fe	0.322	0.808	122.0	This work
2	SPCN/Fe	0.388	0.841	-	
3	CoNP-sIMCOF	0.500	0.830	48	[5]
4	CoO_x@NC-800	0.360	0.890	121.09	[6]
5	CoNP-PTCOF	0.450	0.850	53	[7]
6	CNFs/CoZn-MOF@COF	0.343	0.820	203.6	[8]
7	Bi-COF@MOF-Fe	-	0.867	-	[9]
8	CoFe-CoN@NOALC	0.472	0.820	154	[10]
9	Fe-COF900	-	0.820	-	[11]
10	FeCo@NC	0.440	0.860	265	[12]
11	Fe-SAC@COF	0.290	-	-	[13]
12	FeSA/FeAC@PPy/CC	0.294	0.830	205.1	[14]

References

1. C. F. S. Gupta and E. Yeager, *Journal of Electroanalytical Chemistry*, 1991, **306**, 239-250.
2. Y. Wang, Y. Gao, L. Ma, Y. Xue, Z. H. Liu, H. Cui, N. Zhang and R. Jiang, *ACS Appl Mater Interfaces*, 2023, **15**, 16732-16743.
3. M. G. Park, J. Hwang, Y. P. Deng, D. U. Lee, J. Fu, Y. Hu, M. J. Jang, S. M. Choi, R. Feng, G. Jiang, L. Qian, Q. Ma, L. Yang, Y. S. Jun, M. H. Seo, Z. Bai and Z. Chen, *Adv Mater*, 2024, **36**, e2311105.
4. C. Yang, J. Chen, L. Yan, Y. Gao, J. Ning and Y. Hu, *Applied Catalysis B: Environment and Energy*, 2024, **352**.
5. J.-M. Ju, C. H. Lee, J. H. Park, J.-H. Lee, H. Lee, J.-H. Shin, S.-Y. Kwak, S. U. Lee and J.-H. Kim, *ACS Applied Materials & Interfaces*, 2022, **14**, 24404-24414.
6. M. Li, Q. Yang, L. Fan, X. Dai, Z. Kang, R. Wang and D. Sun, *ACS Applied Materials & Interfaces*, 2023, **15**, 39448-39460.
7. J. H. Park, C. H. Lee, J. M. Ju, J. H. Lee, J. Seol, S. U. Lee and J. H. Kim, *Advanced Functional Materials*, 2021, **31**.
8. L. Liu, Q. He, S. Dong, M. Wang, Y. Song, H. Diao and D. Yuan, *Journal of Colloid and Interface Science*, 2024, **666**, 35-46.
9. A. Tao, B. Guo, C. Yu, X. Yang, G. Liu and G. Zeng, *Chemistry – A European Journal*, 2024, **30**.
10. J. Zhang, J. Liu, J. Ran, X. Lin, H. Wang and X. Qiu, *Chinese Chemical Letters*, 2024, DOI: 10.1016/j.cclet.2024.110403.
11. S. Yang, X. Li, T. Tan, J. Mao, Q. Xu, M. Liu, Q. Miao, B. Mei, P. Qiao, S. Gu, F. Sun, J. Ma, G. Zeng and Z. Jiang, *Applied Catalysis B: Environmental and Energy*, 2022, **307**.
12. Z. Chen, J. Jiang, M. Jing, Y. Bai, X. Zhang, W. Deng, Y. Wu, F. Chen, M. Yi, M. Yang, X. Xu, T. Wu, Y. Zhang and X. Wang, *Carbon Neutralization*, 2024, **3**, 689-699.
13. X. Wang, L. Sun, W. Zhou, L. Yang, G. Ren, H. Wu and W.-Q. Deng, *Cell Reports Physical Science*, 2022, **3**.
14. Q. Liu, P. Qiao, D. Shen, Y. Xie, B. Wang, T. Han, H. Shi, L. Wang and H. Fu, *Energy & Environmental Science*, 2025, **18**, 2839-2851.